Analysis of jet oscillations with acoustic radiation in the recorder by direct aeroacoustic simulations

Kimie Onogi, Hiroshi Yokoyama, and Akiyoshi Iida

Citation: The Journal of the Acoustical Society of America **146**, 1427 (2019); doi: 10.1121/1.5124001
View online: https://doi.org/10.1121/1.5124001
View Table of Contents: https://asa.scitation.org/toc/jas/146/2
Published by the Acoustical Society of America

Analysis of jet oscillations with acoustic radiation in the recorder by direct aeroacoustic simulations

Kimie Onogi, Hiroshi Yokoyama,[a] and Akiyoshi Iida
Department of Mechanical Engineering, Toyohashi University of Technology, 441-8580, Aichi, Japan

(Received 3 April 2019; revised 8 August 2019; accepted 9 August 2019; published online 28 August 2019)

To elucidate the selection mechanism of a predominant mode in acoustic radiation from the recorder, the jet oscillations predicted by direct aeroacoustic simulations are analyzed based on a proposed formula for hydrodynamic and acoustic jet displacements. The displacements are well represented by the formula, taking into account the non-zero initial amplitude around the windway exit and variations of oscillation center with streamwise position for jet displacement. The analysis is applied to the jet oscillations in two different recorders with a straight- and an arch-shaped windway, where the shift of the predominant mode from the first to the second mode occurs for the straight-shaped recorder at a lower jet velocity compared to the arch-shaped recorder. The analytical results present the influence of the recorder shape on the amplification rate of the hydrodynamic jet displacement, the acoustic feedback effects and the phase relation between the hydrodynamic jet displacement and acoustic pressure in the resonator, along with the jet offset to the edge. Compared to the arch-shaped recorder, the convex curve of the amplification rate with the non-dimensional frequency based on the windway height for the straight-shaped recorder is located in the higher-frequency region, which contributes to the predominance of the higher mode.
 https://doi.org/10.1121/1.5124001

[TRM] Pages: 1427–1437

I. INTRODUCTION

In air-reed (flue) instruments, such as the flute and the recorder, a thin air jet is emitted from a windway (channel) exit. The oscillating jet travels across an opening (mouth) in the resonator (pipe) toward a sharp edge (labium). The jet oscillations around the edge induce an unsteady aerodynamic force, which drives the acoustic oscillations in the resonator.[1] The acoustic particle velocity fluctuations at the windway exit induce a modulation of the vorticity in the shear layers of the jet as acoustic feedback. Then, the feedback loop for the acoustic resonance of the instrument is formed.[1]

To understand the oscillations in air-reed instruments, formulas for the jet oscillations have been proposed by several researchers.[2,5–8] The pioneering work by Rayleigh[2] presented an equation for the conservation of vorticity for the oscillating jet, which describes the amplification and convection of the jet oscillations. Michalke[3] and Freymuth[4] experimentally showed that this analysis is appropriate to describe the spatial distributions of the jet oscillations.

Assuming the spatial amplification and convection of the jet oscillations, Fletcher and Thwaites[5,6] proposed a semi-empirical formula, named "the negative displacement model." In this formula, the jet displacement due to the velocity oscillations consists of two components: a convected hydrodynamic displacement spatially developed with an amplification rate, and an acoustic displacement due to the acoustic particle oscillations. This formula assumes that the initial amplitude of jet displacement (jet amplitude) at the windway exit is zero, where the hydrodynamic and the acoustic jet displacements are cancelled out. Verge[7] pointed out that this initial condition is inappropriate and proposed a modified formula of Fletcher's formula,[6] which includes a parameter for fitting the jet displacement at the windway exit. De la Cuadra[8] proposed an empirical formula that includes the non-zero initial jet amplitude, where the initial jet amplitude was estimated by measurement with Schlieren method. The distributions of the amplitude of the velocity fluctuations predicted by this formula fitted well with their experimental results, although the effects of the acoustic jet displacement were not taken into consideration.

Regarding the acoustic power generation due to the jet oscillations, the in-phase relation between the fluctuating jet volume flow into the resonator and the acoustic pressure fluctuations in the resonator is favorable to the acoustic resonance.[9] This relation is consistent with the volume-flow model (Helmholtz–Cremer model)[10–16] that was originally formulated by Cremer and Ising.[15]

In actual musical instruments, the jet oscillations as well as the acoustic radiation depend on the geometry of instuments.[17–20] Ségoufin *et al.*[17] measured the acoustic pressure in organ pipes with different windway lengths, and showed that the windway length affected the amplitude of the acoustic pressure of the second and third harmonics. They also clarified that using chamfers at the end of the long windway resulted in a shorter attack transient and extended the blowing pressure range available for the first acoustic mode. This effect of the chamfer on the attack transient was also confirmed by Giordano[18] by a direct aeroacoustic simulation. Fletcher and Douglas[19] and Yoshikawa[20] calculated the change in the sound pressure levels of harmonics with the

[a]Electronic mail: h-yokoyama@me.tut.ac.jp

relative height of the symmetry plane of jet from the edge (jet offset). Also, based on a direct aeroacoustic simulation along with experiments, Yokoyama *et al.*[21] showed that the threshold of the jet velocity for a shift in the predominant mode in the acoustic radiation was different between recorders with different geometries around the windway exit and edge. However, the selection mechanism of a predominant mode has not been sufficiently investigated.

To elucidate the selection mechanism of a predominant mode in acoustic radiation from an air-reed instrument, this study proposes a modified formula representing the displacement of jet oscillations for each mode based on the flow field predicted by direct aeroacoustic simulations. This formula decomposes the jet oscillations into hydrodynamic and acoustic jet displacements, where the non-zero initial amplitude at the windway exit and the variable oscillation center with the streamwise direction for the jet displacement are taken into account. Based on this formula, this study analyzes the jet oscillations for the first and second modes in two different recorders,[21] one with a straight- and one with an arch-shaped windway.

In Sec. II, the geometries and radiated sound of the recorders are presented. In Sec. III, the numerical methods and the proposed formula for jet displacement are described. In Sec. IV, jet offset from the edge, the phase relation between the jet displacement and the acoustic pressure oscillations in the resonator, the acoustic feedback effects, and the streamwise amplification of the jet oscillations are discussed. Also, the relevance of these physical quantities to the mode selection mechanism in the two recorders are focused on.

II. FLOW CONDITIONS AND RADAITED SOUND

A. Flow conditions

The flow and acoustic fields around the above-mentioned two different recorders were analyzed based on the results of direct aeroacoustic simulations. To reduce the computational cost, a short resonator with three opened tone holes, as shown in Fig. 1, was utilized. The resonator length was $L = 198$ mm for both the recorders. It is noted that these configurations were the same as those in the experimental and computational investigation in our previous paper.[21]

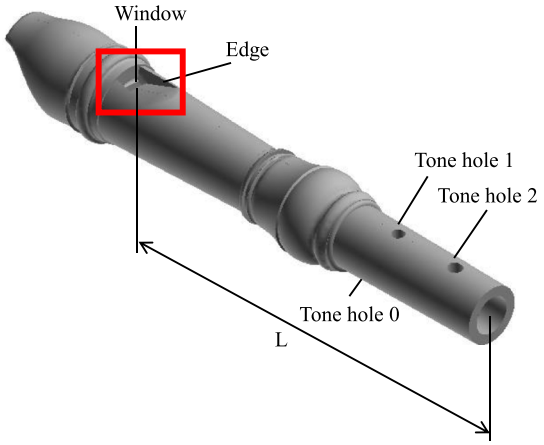

FIG. 1. (Color online) Short recorder with three tone holes.

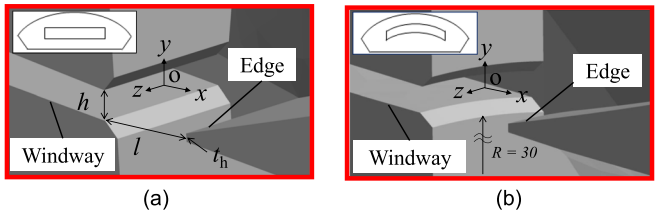

FIG. 2. (Color online) Close-up around windway exit and edge. (a) Straight-shaped recorder. (b) Arch-shaped recorder.

The main difference between the two recorders were the geometries around the windway exit and the edge. As shown in Fig. 2, the recorders had a straight- and an arch-shaped windway exit and edge, and were called the straight- and arch-shaped recorder, respectively. The dimensions of the windway exit height, h, window distance from the windway exit to the edge, l, and the edge position, y_e, are shown in Table I. The origin of the coordinate system was located at the center of the windway exit that is the starting point of the chamfering. The streamwise direction was the x axis, the vertical direction was the y axis, and the spanwise direction intersecting with those two axes was the z-axis.

Simulations were performed under conditions of 10 m/s $\leq U_0 \leq$ 65 m/s, where U_0 is the cross-sectional averaged streamwise velocity at the windway exit ($x = 0$). While the first mode was predominant in the sound pressure levels for both recorders at 20 m/s, the first and second modes were found to be predominant in the arch- and straight-shaped recorders at 35 m/s, respectively.[21] The results at 20 m/s and 35 m/s are mainly discussed in this paper. Reynolds number ($\mathrm{Re} \equiv U_0 h/\nu$) is shown in Table II, where ν is kinematic viscosity.

Figure 3 shows the profiles of time-averaged streamwise velocity U at the spanwise center of the windway exit ($x = 0$, $z = 0$), where the values are non-dimensionalized by its maximum value along the vertical direction, $U_{0,\max}$. The velocity profiles for recorders were similar. The peak of each profile with the marker in Fig. 3 was obtained by fitting a polynomial to the profile. This study defined jet displacement as the instantaneous position of the peak of the velocity profile.

B. Radiated sound

The radiated sound pressure spectra were measured at a distance of 90 mm from the window exit ($x = 0$ mm, $y = 90$ mm, $z = 0$ mm) as shown in Fig. 4. The predicted sound pressure spectra by the direct aeroacoustic simulations[21] at $U_0 = 20$ m/s and 35 m/s are as shown in Fig. 5. The frequency resolution was 78 Hz. At both 20 and 35 m/s, the sound pressure levels (SPL) for the first mode (half-wavelength acoustic mode) around 800 Hz were almost the same for the two recorders, while the level for the second mode (one-wavelength acoustic mode)

TABLE I. Dimensions of recorders, where t_h is the edge thickness.

Recorder	Windway exit height h/t_h	Window distance l/h	Edge position y_e/h
Straight	3.67	4.08	−0.269
Arch	3.04	4.59	−0.374

TABLE II. Reynolds number of recorders.

	Reynolds number Re $\equiv U_0 h/\nu$	
U_0 [m/s]	Straight	Arch
20	1699	1407
35	2974	2463

around 1600 Hz was more intense in the straight-shaped recorder than that in the arch-shaped recorder. At $U_0 = 35$ m/s, the levels of the first and second modes were comparable, and multi-mode resonance occurred in both the recorders. Particularly, in the straight-shaped recorder, the level for the second mode was more intense than that for the first mode, where the acoustic radiation for the second mode became predominant. In this current work, the sound pressure levels at about twice as high as a frequency of the first mode were discussed as the second mode. The sound pressure level at this frequency was confirmed to have distributions of one-wavelength mode in the resonator corresponding to the second mode. However, the exact distinction between the second acoustical mode and the second harmonic of the first mode might be a problem for future study.

To determine which of the shapes around the windway and the dimensions contributed more to the difference in the predominant mode, a preliminary simulation was performed using a recorder called P-arch model, under the condition of $U_0 = 35$ m/s. This recorder model has the arch-shaped windway and edge as in the arch-shaped recorder, while the dimensions (i.e., edge height, windway exit height and window distance) are the same as those of the straight-shaped recorder. As shown in Fig. 5(b), the sound pressure levels of the first and second modes for P-arch recorder were almost the same as those for the arch-shaped recorder, while the level of the second mode was visibly lower than that for the straight-shaped recorder. The reduction of the sound pressure level of the second mode in P-arch recorder indicates that the shapes around the windway and edge mainly contributed to the difference in the predominant mode rather than the dimensions including the edge height. The selection mechanism of the predominant mode due to the shapes is discussed in Sec. IV.

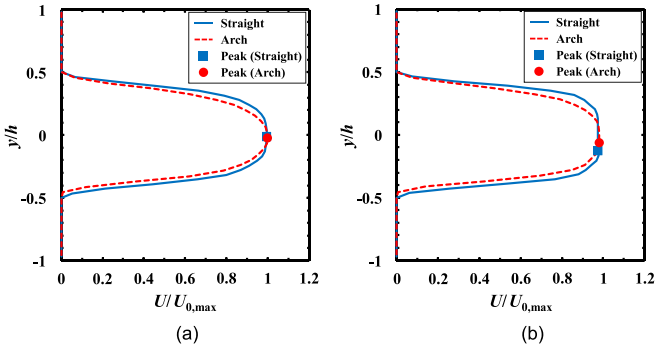

FIG. 3. (Color online) Profiles of time-averaged streamwise velocity at the spanwise center of the windway exit ($x = 0$, $z = 0$). (a) $U_0 = 20$ m/s. (b) $U_0 = 35$ m/s.

III. METHODOLOGIES FOR ANALYSIS OF JET OSCILLATIONS

A. Computational methodologies and validation

1. Governing equations and finite-difference formulation

The governing equations for the simulations of the interactions between the flow and acoustic fields were based on the continuity equation, the three-dimensional compressible Navier–Stokes equations, and the energy conservation equation. A volume-penalization (VP) method,[23,24] which is a type of immersed-boundary method,[25] was used to reproduce the complex shapes of the recorder on a rectangular grid. The governing equations were expressed as follows:

$$\boldsymbol{Q}_t + (\boldsymbol{F}_x - \boldsymbol{G}_x)_x + (\boldsymbol{F}_y - \boldsymbol{G}_y)_y + (\boldsymbol{F}_z - \boldsymbol{G}_z)_z = \boldsymbol{V}, \quad (1)$$

where $\boldsymbol{Q}$ is the vector of the conservative variables, $\boldsymbol{F}$ is the inviscid flux vectors, $\boldsymbol{G}$ is the viscous flux vectors, $\boldsymbol{V}$ is the penalizatin term as follows:

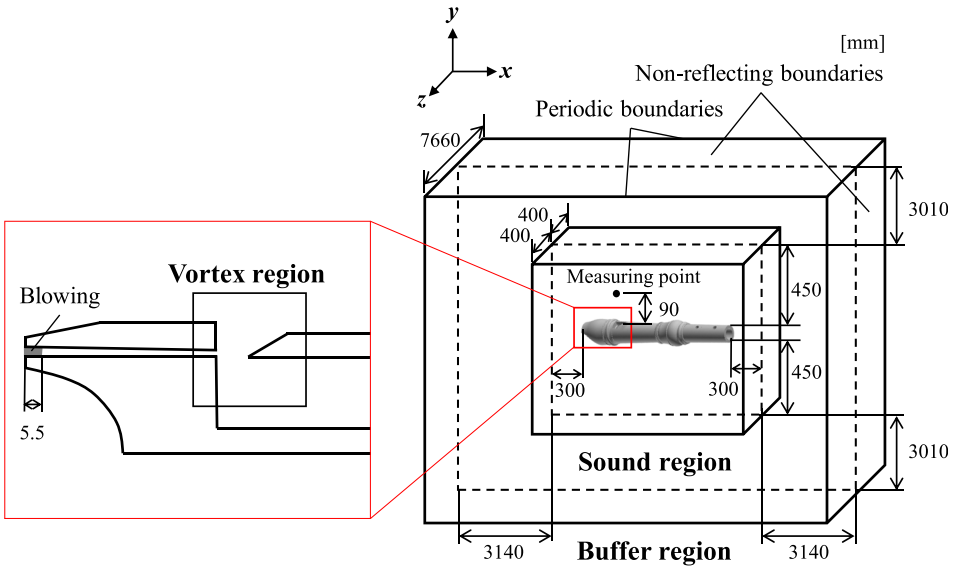

FIG. 4. (Color online) Computational domain and boundary conditions.

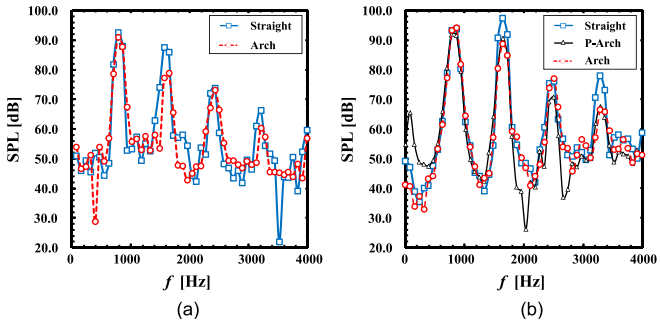

FIG. 5. (Color online) Sound pressure spectra ($x = 0$ mm, $y = 90$ mm, $z = 0$ mm). (a) $U_0 = 20$ m/s. (b) $U_0 = 35$ m/s.

$$\boldsymbol{V} = -\left(\frac{1}{\phi} - 1\right)\chi \begin{pmatrix} \partial \rho u_i / \partial x_i \\ 0 \\ 0 \\ 0 \end{pmatrix}, \quad \phi = 0.25, \tag{2}$$

where the value of ϕ was adjusted to be 0.25 so that the sound could be approximately perfectly reflected on the objects without computational unsteadiness, and χ was the mask function as follows:

$$\chi = \begin{cases} 1 \ (\text{inside object}) \\ 0 \ (\text{outside object}). \end{cases} \tag{3}$$

Spatial derivatives were evaluated by the sixth-order compact finite-difference scheme (fourth-order accuracy at boundaries).[26] Time integration was performed by the third-order Runge–Kutta method.[27]

To reduce numerical instability,[28] the following 10th-order spatial filter was used

$$\alpha_f \hat{\psi}_{i-1} + \hat{\psi}_i + \alpha_f \hat{\psi}_{i+1} = \sum_{n=0}^{5} \frac{\beta_n}{2}\left(\hat{\psi}_{i+n} + \hat{\psi}_{i-n}\right), \tag{4}$$

where ψ and $\hat{\psi}$ are a conservative and a filtered quantity, respectively. Coefficient β_n had the same value as that used by Gaitonde and Visbal,[29] and the value of α_f is 0.45.

2. Computational grid

The computational domain, shown in Fig. 4, was divided into three regions: a vortex region, a sound region, and a buffer region. The computational grid was rectangular (as mentioned above). The grid spacing varied between the regions and was smoothly stretched from the vortex region to the buffer region.

In the vortex region, the minimum grid spacing was set to $\Delta x = \Delta y = 0.05$ mm, $\Delta z = 0.15$ mm around the window exit and the edge, as in our previous paper.[21,22] It has been confirmed that these spacings are sufficiently fine to capture the jet oscillations and vortices around the edge.[22] In the sound region, more than 10 grid points were used per fundamental wavelength to capture the propagation of acoustic waves. In the buffer region, the grid was stretched to attenuate acoustic waves to prevent intense reflections of the acoustic waves on the boundaries.[30] The total number of grid points was approximately 7.7×10^7.

3. Boundary condition and initial conditions

The boundary conditions of the computation are shown in Fig. 4. Non-reflecting boundaries[31–33] were used at the boundaries of the x- and y-directions, and periodic boundary conditions were adopted in the z-direction. To reproduce the jet from the windway, the blowing velocity was set in the inlet region of the windway, as shown in gray color in the left figure of Fig. 4.

4. Validation of computational methods

The above-mentioned computational methods have been validated in our previous paper[21] by comparing the predicted flow field in the jet oscillations with those measured by particle image velocimetry along with the comparison of predicted and measured sound spectra.

Figure 6 shows the predicted and measured variation of the fundamental frequency for the largest sound pressure level (f_p) with the jet velocity U_0 for both the recorders. The predicted fundamental frequencies approximately agreed with those measured for both recorders. Figure 6 also shows that the measured fundamental frequency shifted from the first to second mode around $U_0 = 30, 50$ m/s for the straight- and arch-shaped recorders, respectively. This indicates that the shift to the second mode occurred at a higher jet velocity in the arch-shaped recorder than in the straight-shaped recorder. This feature was correctly predicted by the present simulations as shown in Fig. 6.

B. Modeling of jet oscillations

1. Formula of jet displacement

Fletcher's formula[5] consists of two components of jet displacement: a hydrodynamic jet displacement that is convected and spatially amplified, and an acoustic jet displacement that oscillates due to the acoustic resonance and has an approximately constant amplitude from the windway exit to

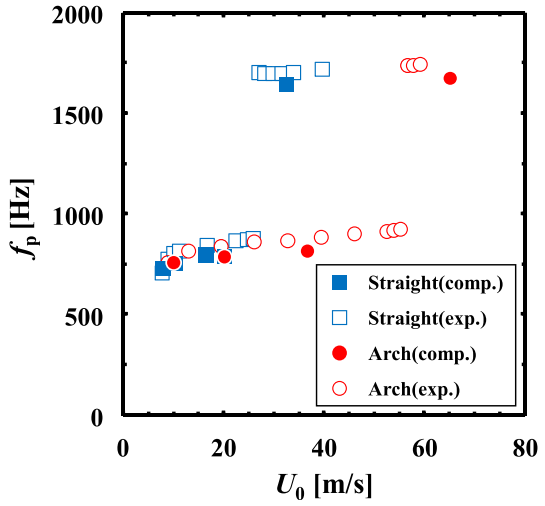

FIG. 6. (Color online) Predicted and measured variation of the fundamental frequency f_p with jet velocity U_0.

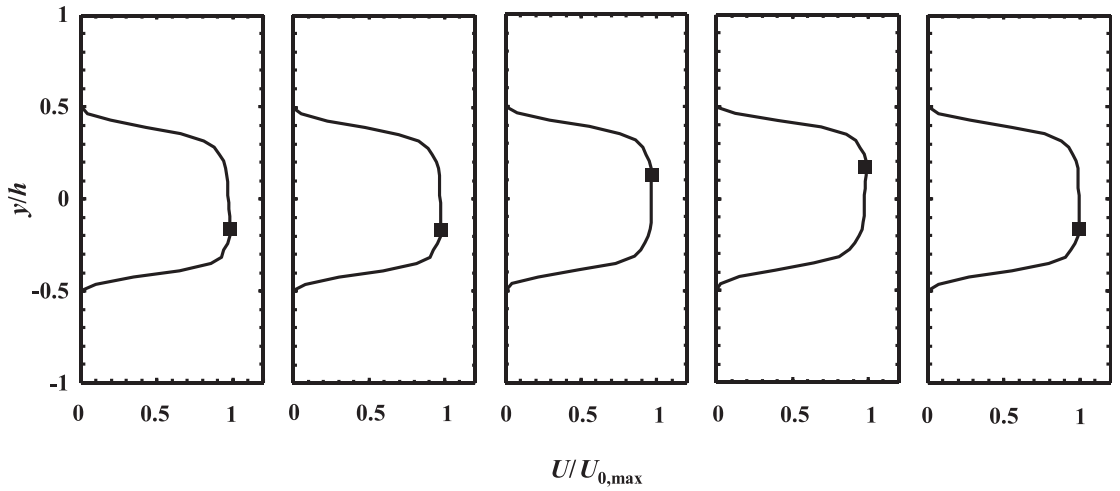

FIG. 7. Time variation of streamwise velocity profile at the spanwise center of the windway exit ($x = 0$, $z = 0$) in the straight-shaped recorder under condition of $U_0 = 35$ m/s at $t/T_1 = 0.2, 0.4, 0.6, 0.8, 1.0$, where T_1 is the fundamental period and $t = 0$ is the instant of expansion in the resonator.

the edge. This formula assumes that the initial jet amplitude at the windway exit ($x = 0$) is zero and that the jet oscillates symmetrically with respect to the center height of the windway exit ($y = 0$). In contrast, our numerical results showed that the jet amplitude at the windway exit was not zero and the center position of the jet oscillations varied with the streamwise position (x). Figure 7 shows the time variation of streamwise velocity profile at the spanwise center of the windway exit ($x = 0$, $z = 0$). The instantaneous position for the peak of each velocity profile changes with time, showing that the jet amplitude at the windway exit is not zero. Figure 8 shows the contours of time-averaged streamwise velocity at the spanwise center ($z = 0$). The center position of the jet varies with the streamwise position. The initial jet amplitude and the spatial variation of the jet center position were observed in each case for both straight- and arch-shaped recorders, under the conditions of $U_0 = 20$, and 35 m/s. Considering the differences between Fletcher's formula[5] and our results, this study proposes a modified formula that better represents the predicted jet oscillations in the simulations.

Assuming that the jet oscillates hydrodynamically and acoustically with the center position varied in the streamwise direction, the jet displacement is expressed as follows:

$$\eta(x,t) = \sum_n \eta_n(x,t) + \bar{\eta}(x) = \sum_n \{\eta_{\mathrm{hydro},n}(x,t) + \eta_{\mathrm{aco},n}(t)\} + \bar{\eta}(x), \tag{5}$$

where $\bar{\eta}(x)$ corresponds to the oscillation center and was computed by averaging the predicted jet displacement during one fundamental period. $\eta_{\mathrm{hydro},n}$ and $\eta_{\mathrm{aco},n}$ are the following hydrodynamic and acoustic jet displacements for the nth mode of jet oscillations, respectively,

$$\eta_{\mathrm{hydro},n}(x,t) = \mathrm{e}^{\alpha_n x}\lambda_{\mathrm{hydro},n}\sin\left[\frac{2\pi}{T_n}\left\{t - \left(t_{\mathrm{c},n}(x) + t_{0,\mathrm{n}} + t_{\mathrm{aco},n} + t_{\mathrm{p},n}\right)\right\} - \frac{\pi}{2}\right], \tag{6}$$

$$\eta_{\mathrm{aco},n}(t) = \lambda_{\mathrm{aco},n}\sin\left[\frac{2\pi}{T_n}\left\{t - \left(t_{\mathrm{aco},n} + t_{\mathrm{p,n}}\right)\right\} - \frac{\pi}{2}\right]. \tag{7}$$

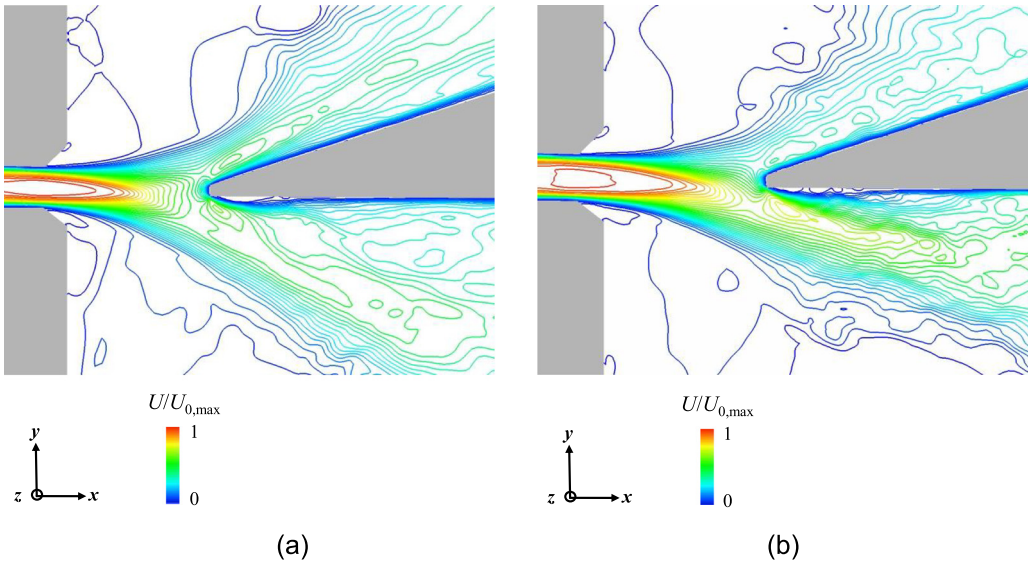

FIG. 8. (Color online) Time-averaged streamwise velocity at the spanwise center ($z = 0$) in the straight-shaped recorder. (a) $U_0 = 20$ m/s. (b) $U_0 = 35$ m/s.

Here α_n and $\lambda_{\mathrm{hydro},n}$ are the streamwise amplification rate and the amplitude of the hydrodynamic jet displacement at the windway exit, respectively, and $\lambda_{\mathrm{aco},n}$ is the amplitude of the acoustic jet displacement. The time period of each mode is represented by T_n. $t_{\mathrm{p},n}$, $t_{\mathrm{aco},n}$, $t_{0,n}$, and $t_{\mathrm{c},n}$ (x) are the time delay of the sound pressure fluctuations in the resonator for the nth mode from that for the first mode ($t_{p,1} = 0$), the time delay of the acoustic jet displacement from the sound pressure fluctuations, the time delay of the hydrodynamic jet displacement from the acoustic jet displacement at the windway exit, and the time delay of the convected hydrodynamic jet displacement at each streamwise position from that at the windway exit ($t_{\mathrm{c},n}(0) = 0$), respectively. The reference time ($t = 0$) is the instant for the lowest value of the sound pressure fluctuations in the resonator for the first mode, where the sound pressure fluctuations for the nth mode were evaluated at the antinode of each mode. This decomposition of jet displacement into the two components allows quantitative analysis of the hydrodynamic jet displacement due to feedback effect from the acoustic oscillation as well as phase relation between hydrodynamic jet displacement and acoustic oscillation.

Regarding the phase relation, the acoustic jet displacement ($\eta_{\mathrm{aco},n}$) was assumed to be in-phase relation with the acoustic particle displacement due to the acoustic resonance around the window referring to Fletcher's formula.[5] To obtain the time delay of the acoustic jet displacement, $t_{\mathrm{aco},n}$, the acoustic particle displacement around the window was estimated by integrating the acoustic particle velocity for each mode, v_{n}, observed in the region close to the windway exit in the mouth field ($x/h \approx 1$, $-7 < y/h < -2$), where the effects of the hydrodynamic jet displacements on the velocity field are negligible.

Compared with Fletcher's formula,[5] the time delay of the hydrodynamic jet displacement to the acoustic jet displacement at the windway exit, $t_{0,n}$, is newly taken into account in this modified formula. In this formula, the convection velocity of hydrodynamic jet displacements, $U_{\mathrm{c},n}$, can vary with streamwise direction. The relation between $t_{\mathrm{c},n}(x)$ and the convection velocity is

$$t_{\mathrm{c},n}(x) = \int_0^x 1/U_{\mathrm{c},n}(s)\mathrm{d}s. \tag{8}$$

2. Estimation of jet parameters

The estimation in this paper utilized the jet displacement at the cross section of the spanwise center ($z = 0$) because the jet behaviors were almost two-dimensional along the spanwise extent of the windway exit. The instantaneous peak height of the velocity profile was fitted as the function of only time t and the streamwise position x. In a preliminary operation, the specific mode of the predicted jet fluctuations was extracted by setting the jet amplitudes of the other modes of the Fourier-transformed jet oscillation to zero and performing an inverse Fourier transformation.

The above-mentioned jet parameters, α_n, $\lambda_{\mathrm{hydro},n}$, $\lambda_{\mathrm{aco},n}$, $t_{0,n}$, and $t_{\mathrm{c},n}(x)$ were obtained by fitting each mode of predicted jet oscillations to Eqs. (5)–(7). First, to obtain the hydrodynamic parameter, $\lambda_{\mathrm{hydro},n}$, the differential jet displacement is expressed as follows:

$$\begin{aligned}\eta_{\mathrm{diff},n}(x,t) &= \eta_n(x,t) - \eta_n(0,t)\\ &= \eta_{\mathrm{hydro},n}(x,t) - \eta_{\mathrm{hydro},n}(0,t),\end{aligned} \tag{9}$$

where the acoustic jet displacement $\eta_{\mathrm{aco},n}$ is canceled out. The amplitude of the differential jet displacement in Eq. (9) is

$$\begin{aligned}\lambda_{\mathrm{diff},n}(x,t) = \Big[&e^{2\alpha_n x}\lambda^2_{\mathrm{hydro},n} - 2e^{\alpha_n x}\lambda^2_{\mathrm{hydro},n}\\ &\times \cos\{2\pi t^*_{\mathrm{c},n}(x)/T_n\} + \lambda^2_{\mathrm{hydro},n}\Big]^{1/2}.\end{aligned} \tag{10}$$

Each parameter was solved by an iteration method, and the initial values for $t^*_{c,n}(x)$ were set using Eq. (8) by assuming $U_{\mathrm{c},n} = 0.4\,U_{0,\max}$.[34] Then α_n and $\lambda_{\mathrm{hydro},n}$ were obtained by fitting the differential jet amplitudes of the numerical results to Eq. (10). Next, $t_{0,n}$ and $\lambda_{\mathrm{aco},n}$ were obtained by fitting the jet displacements of the numerical results at the windway exit to η_n $(0,t)$. After that, $t_{\mathrm{c},n}$ (x) was obtained by fitting the jet displacements at each streamwise position to η_n (x,t). Finally, α_n was corrected by fitting the jet amplitudes of the numerical results to the numerical expression for the jet amplitude:

$$\begin{aligned}\lambda_n(x,t) = \Big[&e^{2\alpha_n x}\lambda^2_{\mathrm{hydro},n} - 2e^{\alpha_n x}\lambda_{\mathrm{hydro},n}\lambda_{\mathrm{aco},n}\\ &\times \cos\{2\pi(t^*_{\mathrm{c},n}(x) + t_{0,n})/T_n\} + \lambda^2_{\mathrm{aco},n}\Big]^{1/2}.\end{aligned} \tag{11}$$

Using the obtained $t_{\mathrm{c},n}(x)$ and α_n, $\lambda_{\mathrm{hydro},n}$ was corrected using Eq. (10) and the fitting processes were repeated until the change rate of each parameter at nth fitting, $|(a^n - a^{n-1})/a^{\mathrm{n}}|$, was reduced to about 2%.

3. Validation for proposed formula of jet displacement

Figures 9 and 10 show the spatial and temporal variations of the jet displacement for the first and second modes in the straight-shaped recorder at $U_0 = 35$ m/s. The square

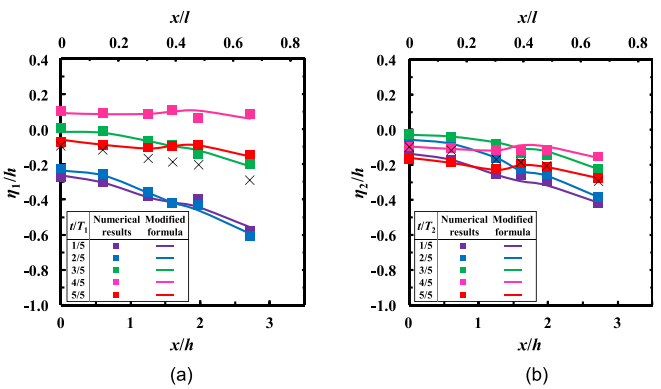

FIG. 9. (Color online) Spatial variations of the jet displacement for the straight-shaped recorder at $U_0 = 35$ m/s, where cross symbols indicate positions of the oscillation center. T_1 and T_2 represent the time periods of the first and second modes. (a) First mode. (b) Second mode.

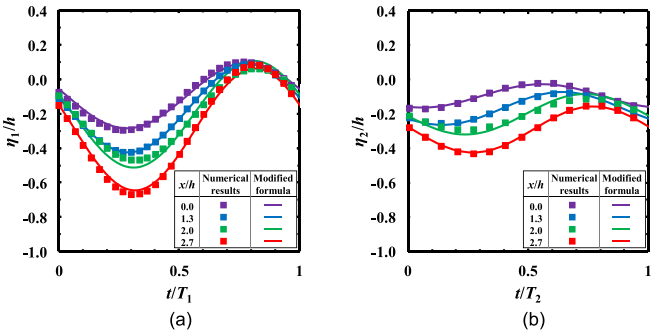

FIG. 10. (Color online) Temporal variation of jet displacement for the straight-shaped recorder at $U_0 = 35$ m/s. T_1 and T_2 represent the time periods of the first and second modes. (a) First mode. (b) Second mode.

symbols show the jet displacement predicted by the direct aeroacoustic simulations. The curves represent the jet displacement based on the proposed formula.

Figure 9 shows that the non-zero jet amplitudes at the windway exit ($x = 0$) were observed and that the position for the oscillation center indicated by the cross symbols varied from zero with the streamwise position (x). This indicates that it is difficult to fit Fletcher's formula[5] to the jet oscillations predicted by the simulations. Figures 9 and 10 show that the spatial and temporal variations of the displacement predicted by the direct aeroacoustic simulations fitted well with the proposed formula. Figure 11 shows the jet amplitude at each streamwise position and the error rate of the numerical results. The averaged error rate is within 10% at almost all points. In Sec. IV, the analytical results for the jet oscillations with the first mode at $U_0 = 20$, and those with the first and second modes at 35 m/s for the straight- and arch-shaped recorders are discussed, where the amplitude of the jet fluctuations for the second mode at $U_0 = 20$ m/s are too small to give an accurate fit to the proposed formula.

IV. ANALYSIS OF JET OSCILLATIONS

A. Jet offset from the edge

Figure 12 shows the variation of the oscillation center of the jet, $\bar{\eta}$, with each streamwise position. The oscillation center became lower from the windway exit to the edge in all cases. This means that the jet deflects towards the resonator.

In both the recorders, the oscillation center below the edge was $\bar{\eta}/h \simeq -0.4$ and -0.5 at $U_0 = 20$ and 35 m/s, respectively. The relative height of the oscillation center of

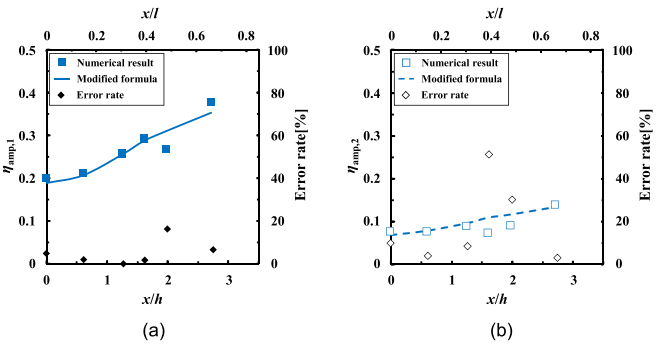

FIG. 11. (Color online) Jet amplitude and error rate in the straight-shaped recorder at $U_0 = 35$ m/s. (a) First mode. (b) Second mode.

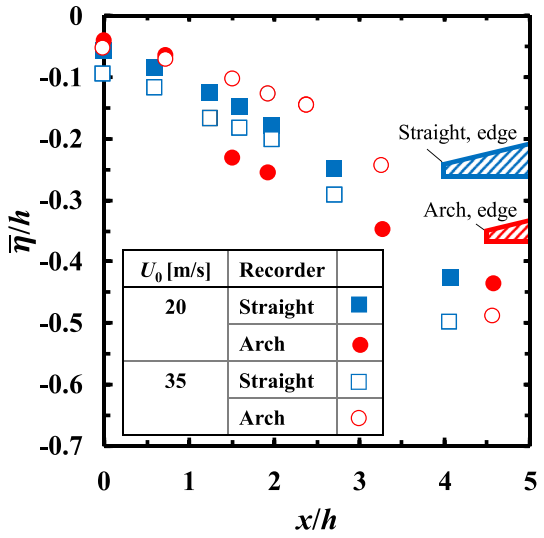

FIG. 12. (Color online) Variation of jet oscillation center with streamwise position.

the jet from the edge (jet offset), e_j, are shown in Table III. Since the edge height was higher in the straight-shaped recorder than in the arch-shaped recorder as shown in Table I, the absolute value of the jet offset, $|e_j/h|$, was about 0.1 larger in the straight-shaped recorder compared to the arch-shaped recorder at both velocities. The theoretical calculations for organ pipes in Refs. 19 and 20 have shown that the second harmonic sound becomes intense with the increase of the jet offset for the range of the jet offset in the present cases ($|e_j/h| < 0.25$). Since the sound pressure levels of the first and second modes for P-arch recorder, which had the same edge height as the straight recorder, were almost the same as for the arch-shaped recorder, as shown in Fig. 5(b), the contribution of the edge height and the resulting $|e_j/h|$ on the difference in the intensification of the radiation in the second mode is not significant.

B. Phase of hydrodynamic and acoustic pressure

Table IV shows the identified jet parameters in Eqs. (5)–(7) including the time delay of the hydrodynamic displacement to the acoustic displacement at the windway exit ($t_{0,n}$). The obtained time delay was in the range of $t_{0,n} = 0.6$–0.75 for all cases. Although the hydrodynamic and acoustic displacement were not completely in the opposite phase, the sign of the hydrodynamic displacement can be opposite compared to that of the acoustic displacement, which supports the generation of negative hydrodynamic jet displacement by acoustic particle displacements at the windway exit, as assumed in Fletcher's formula.[5] Also as seen in

TABLE III. Non-dimensional jet offset.

U_0 [m/s]	Recorder	Jet offset e_j/h
20	Straight	−0.16
	Arch	−0.06
35	Straight	−0.23
	Arch	−0.12

TABLE IV. Non-dimensional jet parameters in Eqs. (5)–(7).

U_0 [m/s]	Recorder	Mode n	Hydrodynamic jet displacement ($x=0$) Amplitude $\lambda_{\mathrm{hydro},n}/h$	Hydrodynamic jet displacement ($x=0$) Time delay to acoustic displacement $t_{0,n}/T_n$	Acoustic jet displacement ($x=0$) Amplitude $\lambda_{\mathrm{aco},n}/h$
20	Straight	1	0.118	0.653	0.103
	Arch	1	0.070	0.608	0.081
35	Straight	1	0.093	0.750	0.166
		2	0.071	0.708	0.015
	Arch	1	0.075	0.750	0.067
		2	0.042	0.675	0.001

Table IV, at the windway exit, the amplitude of the acoustic displacement, $\lambda_{\mathrm{aco},n}$, can be comparable to that of the hydrodynamic displacement, $\lambda_{\mathrm{hydro},n}$, which indicates that the acoustic displacement is not negligible. The appropriate evaluation of the acoustic components leads to the reasonable convection velocity discussed in the next paragraph.

The convection velocities of the fluctuations in the jet, $U_{\mathrm{c},n}$, around the center between the windway exit and edge ($x/h=2.0$) were calculated by the convective time of the hydrodynamic jet displacement from the windway exit to a downstream point, $t_{\mathrm{c},n}$ (x), based on Eq. (8). Table V shows that the nondimensionalized convection velocities, $U_{\mathrm{c},n}/U_{0,\max}$, varied from 0.4 to 0.65 for all cases. These values were almost within the range of the convection velocities measured in Refs. 8 and 34, which indicates that the present formula for the jet displacement is appropriate.

The phase difference between the hydrodynamic displacement of the jet near the edge and the acoustic pressure in the resonator, where the phase difference affects the threshold for the acoustic power generation[10] and the anti-phase relation is regarded as favorable,[9] was estimated by $-(t_{\mathrm{c},n}(l)+t_{0,n}+t_{\mathrm{aco},n})/T_n$ and is shown in Table VI. The phase difference varied from 0.33 to 0.52 for both the first and second modes in both the recorders at $U_0=35$ m/s, where this range is within the threshold for the acoustic power generation of 0.25–0.75.[10] (See Table VI.) This is possibly related with the multi-mode resonance for both the straight- and arch-shaped recorders at $U_0=35$ m/s, as shown in Fig. 5.

C. Acoustic feedback effects

The acoustic feedback effects on the jet, which are induced by the acoustic particle velocity oscillations,[1] were evaluated based on the ratio of the amplitude of the hydrodynamic displacement (hydrodynamic jet amplitude) at the windway exit to the amplitude of the acoustic particle displacement, $|\lambda_{\mathrm{hydro},n}/\left(\sqrt{2}v_{\mathrm{RMS},n}/\omega_n\right)|$, where ω_n is the angular frequency of each mode. The acoustic particle displacement was estimated by the above-mentioned acoustic particle velocity near the window, v_n.

Figure 13 shows the variation of ratio of the hydrodynamic jet amplitude to the acoustic particle displacement, $|e^{\alpha_n x}\lambda_{\mathrm{hydro},n}/\left(\sqrt{2}v_{\mathrm{RMS},n}/\omega_n\right)|$, with the streamwise position. Figure 13 shows that the ratio at the windway exit for each mode and each jet velocity was almost the same for both recorders. This indicates that the influence of the shape difference between the straight- and arch-shaped recorders on the acoustic feedback effects are small. This is possibly because almost the same jet velocity profile was formed in each recorder, as shown in Fig. 3, where the profile can affect the acoustic feedback.[8,17,35]

D. Amplification of jet oscillations with convection

Figure 14 shows the amplitude of displacement fluctuations in the second mode normalized by that in the first mode at the streamwise position of the edge ($x/l=1.0$), where the values include both the hydrodynamic and the acoustic jet displacement. It was found that the normalized jet amplitude for the second mode was larger in the straight-shaped recorder compared to the arch-shaped recorder. This relative intensification of the jet displacement fluctuations for the second mode in the straight-shaped recorder promotes the relative intensification of the acoustic power generation for the second mode and contributes to the predominance of the acoustic radiation for the second mode.

Figure 15 shows the variation of the hydrodynamic jet amplitude with the streamwise direction for both straight- and arch-shaped recorders, where the amplitude was non-dimensionalized by the windway exit height, h. The

TABLE V. Non-dimensional convection velocity around $x/h=2.0$, where values are non-dimensionalized by the maximum jet velocity at windway exit.

U_0 [m/s]	Recorder	Mode n	Convection velocity $U_{\mathrm{c},n}/U_{0,\max}$
20	Straight	1	0.545
	Arch	1	0.502
35	Straight	1	0.569
		2	0.640
	Arch	1	0.435
		2	0.566

TABLE VI. Phase difference of hydrodynamic jet displacement at edge from acoustic pressure.

U_0 [m/s]	Recorder	Mode n	Phase difference $-(t_{\mathrm{c},n}(l)+t_{0,n}+t_{\mathrm{aco},n})/T_n$
20	Straight	1	0.36
	Arch	1	0.33
35	Straight	1	0.34
		2	0.52
	Arch	1	0.33
		2	0.48

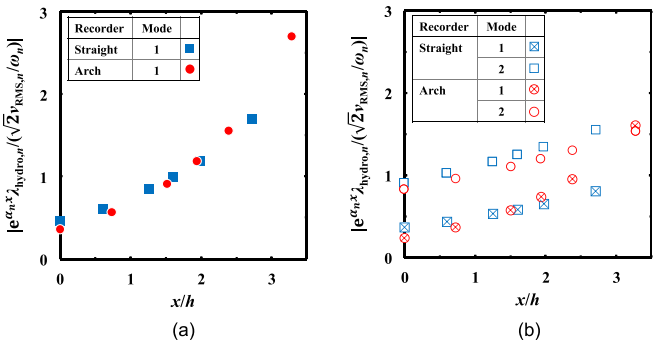

FIG. 13. (Color online) Variation of amplitude of hydrodynamic jet displacement, where the values are non-dimensionalized by acoustic particle displacement around the window. (a) $U_0 = 20$ m/s. (b) $U_0 = 35$ m/s.

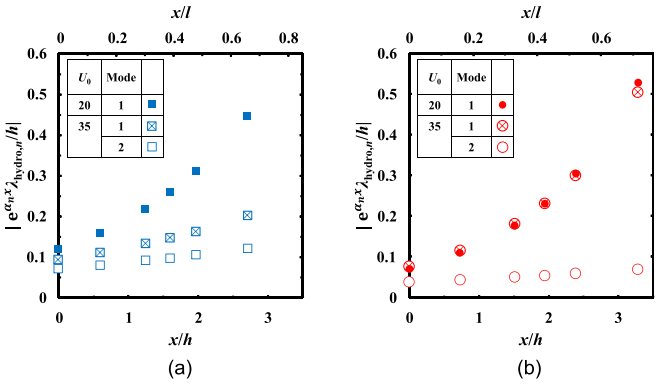

FIG. 15. (Color online) Variation of hydrodynamic jet amplitude in the streamwise position. (a) Straight-shaped recorder. (b) Arch-shaped recorder.

hydrodynamic jet amplitude of the first mode in the downstream became smaller as the velocity increases from $U_0 = 20$ to 35 m/s. Particularly, the decrease was more drastic in the straight-shaped recorder compared to the arch-shaped recorder. At $U_0 = 35$ m/s, the hydrodynamic jet amplitude for the first mode became relatively close to that for the second mode in the straight-shaped recorder, while that for the first mode was still significantly larger than that for the second mode in the arch-shaped recorder. As a result, the relative intensification of the jet displacement fluctuations for the second mode compared to those for the first mode is promoted more in the straight-shaped recorder, as shown in Fig. 14.

The hydrodynamic jet amplitude grows in the streamwise direction with the amplification rate, α. Figure 16 shows the relation between the amplification rate and the non-dimensional frequency $\mathrm{Str}_h \equiv f_p h/U_{0,\max}$. Theoretical analysis[35] and experiments[8] have shown that the relation is represented by a convex curve. The curve for each recorder was given its own color (one was blue and one was red), and each curve had three data points. Compared with the arch-shaped recorder, the convex curve for the straight-shaped recorder was located in a higher-frequency region. This means that the peak of α for the straight-shaped recorder appears at the lower jet velocity for each mode. This leads to the above-mentioned drastic decrease of the amplification rate for the first mode in the straight-shaped recorder when increasing the velocity from 20 to 35 m/s. As a result, the relative jet amplitude for the second normalized by that for the first mode increases more significantly in the straight-shaped recorder compared to the arch-shaped recorder as shown in Fig. 14.

The relation between the amplification rate, α, and the non-dimensional frequency, Str_h, in flute-like instruments with different windway lengths and chamfers was also investigated by de la Cuadra.[8] The experiments showed that the relation did not depend on the windway length but the chamfer geometry. The geometrical differences of windway exit (straight- or arch-shaped) probably causes the difference in the amplification rate of the jets between the recorders. This can lead to the difference of intensity in the jet fluctuations and acoustic radiation of each mode for the two recorders.

The effects of geometric difference were quantitatively evaluated by introducing the modified formula that is consistent with the jet oscillations predicted by the direct aeroacoustic simulations. The proposed analysis along with the direct aeroacoustic simulations requires large computational efforts. However, the present analysis of the jet oscillations can also be applied to experimental data.

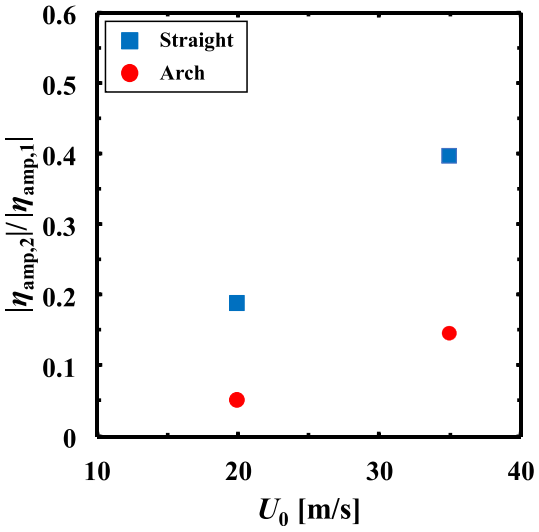

FIG. 14. (Color online) Amplitude of jet displacement in the second mode normalized by that in the first mode ($x/l = 1.0$).

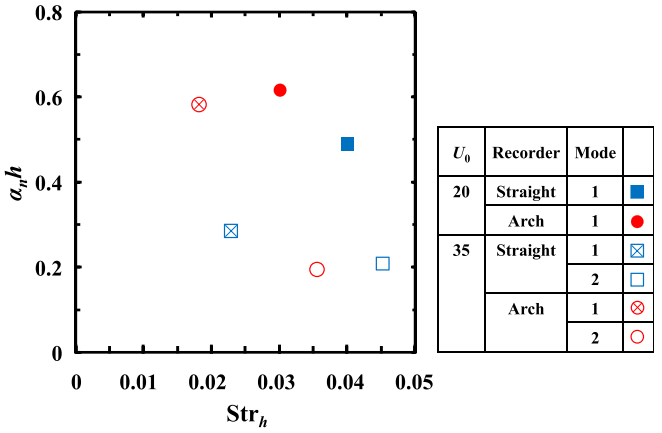

FIG. 16. (Color online) Relation between the streamwise amplification rate and the non-dimensional frequency, Str_h.

V. CONCLUSION

To elucidate the selection mechanism of a predominant mode in acoustic radiation with the first and second modes from two different recorders, one with a straight- and one with an arch-shaped windway, the proposed formula for hydrodynamic and acoustic jet displacements was applied to an analysis of the jet oscillations predicted by direct aeroacoustic simulations.

The computational results showed the non-zero initial jet amplitude at the windway exit and the deflection of the oscillation center of the jet towards the resonator in the downstream. With these taken into account, the spatial and temporal variation of the jet displacement predicted by the simulations are represented well by the proposed formula.

Since sound pressure level (SPL) of the first and second modes for a recorder that has the arch-shaped windway and the same edge height as the straight recorder were almost the same as those for the arch-shaped recorder, the contribution of the difference in the jet offset from the edge to the difference in the intensification of the radiation in the second mode was found not to be significant.

The acoustic feedback effects were estimated based on the ratio of the amplitude of the hydrodynamic displacement to the acoustic particle displacement around the window. The analysis demonstrated that the influence of the shape difference of the two recorders on the acoustic feedback effects is small, where the velocity profile of the jet at the windway exit was almost the same for both recorders.

The amplification rate of the hydrodynamic displacement along the streamwise direction was also estimated for each mode of the two recorders. It was shown that the convex curve of the amplification rate with the non-dimensional frequency based on the windway exit height for the straight-shaped recorder was located on a higher-frequency region than that for the arch-shaped recorder. This leads to the drastic decrease of the amplification rate for the first mode of the straight-shape recorder when increasing the jet velocity from 20 to 35 m/s, which eventually promotes the relative intensification of the acoustic power generation for the second mode to the first mode in the straight-shaped recorder.

In both recorders, the phase difference between the hydrodynamic displacement and the acoustic pressure fluctuations in the resonator was within the range of the threshold for the acoustic power generation for both the first and second modes at the jet velocity of 35 m/s. This supports the acoustic radiation with the multi-mode resonance predicted by the direct aeroacoustic simulations.

In actual musical instruments, differences in shape can affect the mode selection mechanism, as shown in this paper. The application of the analytical methodologies proposed in this paper can provide an effective means to elucidate the mode selection mechanism in air-reed instruments.

ACKNOWLEDGMENTS

We would like to thank T. Shoji, K. Arimoto, S. Usa, A. Miki, and H. Onitsuka from YAMAHA Corporation for sharing the experimental data and useful discussions. This work was supported by JSPS KAKENHI Grant Number 17K06153 and through the Application development for Post K computer (FLAGSHIP 2020) by the Ministry of Education, Culture, Sports, Science, and Technology of Japan (MEXT).

[1]B. Fabre, J. Gilbert, A. Hirschberg, and X. Pelorson, "Aeroacoustics of musical instruments," Ann. Rev. Fluid Mech. **44**, 1–25 (2012).
[2]L. Rayleigh (J. W. Strutt), *The Theory of Sound* (Dover, New York, 1945), Vol. 2, Chap. 21.
[3]A. Michalke, "On spatially growing disturbances in an inviscid shear layer," J. Fluid Mech. **23**, 521–544 (1965).
[4]P. Freymuth, "On transition in a separated laminar boundary layer," J. Fluid Mech. **25**, 683–704 (1966).
[5]N. H. Fletcher, "Sound production by organ flue pipes," J. Acoust. Soc. Am. **60**(4), 926–936 (1976).
[6]N. H. Fletcher and S. Thwaites, "Wave propagation on an acoustically perturbed jet," Acustica **42**(5), 323–334 (1979).
[7]M. P. Verge, "Aeroacoustics of confined jets: With application to the physical modeling of recorder-like instruments," Ph.D. thesis, Eindhoven University of Technology, 1995.
[8]P. de la Cuadra, "The sound of oscillating air jets: Physics, modeling and simulation in flute-like instruments," Ph.D. thesis, Stanford University, 2005.
[9]S. Yoshikawa, H. Tashiro, and Y. Sakamoto, "Experimental examination of vortex-sound generation in an organ pipe: A proposal of jet vortex-layer formation model," J. Sound Vib. **331**, 2558–2577 (2012).
[10]N. H. Fletcher and T. D. Rossing, *The Physics of Musical Instruments*, 2nd ed. (Springer Verlag, New York, 1998).
[11]J. W. Coltman, "Sounding mechanism of the flute and organ pipe," J. Acoust. Soc. Am. **44**, 983–992 (1968).
[12]J. W. Coltman, "Jet drive mechanism in edge tones and organ pipes," J. Acoust. Soc. Am. **60**, 725–733 (1976).
[13]S. A. Elder, "On the mechanism of sound production in organ pipes," J. Acoust. Soc. Am. **54**, 1554–1564 (1973).
[14]N. H. Fletcher, "Jet drive mechanism in organ pipes," J. Acoust. Soc. Am. **60**, 481–483 (1976).
[15]L. Cremer and H. Ising, "Die selbsterregten Schwingungen von Orgelpfeifen" ("The self-excited vibrations of organ pipes)," Acustica **19**(3), 143–153 (1967).
[16]S. Yoshikawa and J. Saneyoshi, "Feedback excitation mechanism in organ pipes," J. Acoust. Soc. Jpn. (E) **1**, 175–191 (1980).
[17]C. Ségoufin, B. Fabre, M. P. Verge, A. Hirschberg, and A. P. J. Wijnands, "experimental study of the influence of the mouth geometry on sound production in a recorder-like instrument: Windway length and chamfers," Acust. Acta Acust. **86**, 649–661 (2000).
[18]N. Giordano, "Simulation studies of a recorder in three dimensions," J. Acoust. Soc. Am. **135**(2), 906–916 (2014).
[19]N. H. Fletcher and Lorna M. Douglas, "Harmonic generation in organ pipes, recorders, and flutes," J. Acoust. Soc. Am. **68**(3), 767–771 (1980).
[20]S. Yoshikawa, "Harmonic generation mechanism in organ pipes," J. Acoust. Soc. Jpn. (E)**5**, 1, 17–29 (1984).
[21]H. Yokoyama, R. Hamasuna, A. Miki, H. Onitsuka, and A. Iida, "Direct aeroacoustic simulation related with mode change in a recorder," in *Proceedings of European Congress on Computational Methods in Applied Sciences and Engineering* (2016), pp. 1315–1324.
[22]H. Yokoyama, A. Miki, H. Onitsuka, and A. Iida, "Direct numerical simulation of fluid−acoustic interactions in a recorder with tone holes," J. Acoust. Soc. Am. **138**, 858–873 (2015).
[23]P. Angot, C. H. Bruneau, and P. Frabrie, "A penalization method to take into account obstacles in viscous flows," Numer. Math. **81**, 497–520 (1999).
[24]Q. Liu and O. V. Vasilyev, "A Brinkman penalization method for compressible flows in complex geometries," J. Comp. Phys. **227**, 946–966 (2007).
[25]R. Mittal and G. Iaccarino, "Immersed boundary methods," Annu. Rev. Fluid Mech. **37**, 239–261 (2005).
[26]S. K. Lele, "Compact finite difference schemes with spectral-like resolution," J. Comp. Phys. **103**, 16–19 (1992).
[27]A. Jameson and T. J. Baker, "Solution of the Euler equations for complex configurations," AIAA Paper 83-1929.
[28]K. Matsuura and C. Kato, "Large-eddy simulation of compressible transitional flows in a low-pressure turbine cascade," AIAA J. **45**, 442–457 (2007).
[29]D. V. Gaitonde and M. R. Visbal, "Pade-type higher-order boundary filters for the Navier-Stokes equations," AIAA J. **38**, 2103–2112 (2000).

[30]T. Colonius,T. S. K. Lele, and P. Moin, "Boundary conditions for direct computation of aerodynamic sound generation," AIAA J. **31**(9), 1574–1582 (1993).
[31]K. W. Thompson, "Time dependent boundary conditions for hyperbolic systems," J. Comp. Phys. **68**, 1–24 (1987).
[32]T. J. Poinsot and S. K. Lele, "Boundary conditions for direct simulations of compressible viscous flows," J. Comp. Phys. **101**, 104–129 (1992).
[33]J. W. Kim and D. J. Lee, "Generalized characteristic boundary conditions for computational aeroacoustics," AIAA J. **38**(11), 2040–2049 (2000).
[34]S. Yoshikawa, "Jet-wave amplification in organ pipes," J. Acoust. Soc. Am. **103**(5), 2706–2717 (1998).
[35]G. E. Mattingly and W. O. Criminale, "Disturbance characteristics in a plane jet," Phys. Fluids **14**(11), 2258–2264 (1971).